Carbohydrate Polymers 84 (2011) 383–389

Contents lists available at ScienceDirect

Carbohydrate Polymers

journal homepage: www.elsevier.com/locate/carbpol

Green composite films composed of nanocrystalline cellulose and a cellulose matrix regenerated from functionalized ionic liquid solution

Hao Ma [a], Bo Zhou [a], Hong-Sheng Li [a], Yi-Qun Li [a,*], Shi-Yi Ou [b]

[a] Department of Chemistry, Jinan University, Guangzhou 510632, China
[b] Department of Food Science & Engineering, Jinan University, Guangzhou 510632, China

ARTICLE INFO

Article history:
Received 29 September 2010
Received in revised form
19 November 2010
Accepted 20 November 2010
Available online 26 November 2010

Keywords:
All-cellulose films
Nanocomposite
Nanoparticle-reinforced composites
Mechanical properties
Ionic liquid

ABSTRACT

By using the excellent selective solubility of the hydroxyl functionalized ionic liquid, 1-(2-hydroxylethyl)-3-methyl imidazolium chloride ([HeMIM]Cl), to the pretreated microcrystalline cellulose (PMCC) and nanocrystalline cellulose (NCC), a green all-cellulose nanocomposite film, in which both the fibers and the matrix are cellulose, was easily prepared *via* adding NCC to the cellulose ionic liquid solution. It was found that the PMCC can be efficiently dissolved in [HeMIM]Cl, whereas NCC slightly dissolved in it. The morphology, crystalline structure, thermal stabilities, mechanical and optical properties of the as-prepared film were characterized by X-ray diffraction (XRD), thermal gravimetric analysis (TGA), scanning electron microscope (SEM), optical transmittance and mechanical testing. The nanocomposite films showed good optical transparency, thermal stabilities and mechanical properties as the result of reinforcement by increasing the content of NCC. But, with the content of NCC increased from 5% to 25%, the decomposition temperature and elongation at break decreased obviously. This work demonstrated a promising route for the preparation of biodegradable green all-cellulose nanocomposites. In addition, this all-cellulose nanocomposite composite is composed of sustainable biodegradable resources, which give it to be benign to environment.

1. Introduction

Cellulose is a very important renewable resource on the earth and regaining importance as renewable chemical resources to replace petroleum-based materials (Schurz, 1999). It can be converted into cellulose derivatives and regenerated materials, which takes an important part in our daily life for its use in furniture, clothing, packaging, paper, and medical products (Fink, Weigel, Purz, & Ganster, 2001). In recent years, biodegradable and plant-derived composites designated as "green" composites have drawn much attentions due to its unique properties such as excellent transparency, mechanical properties and nontoxic (Takagi & Asano, 2008). In recent years, the "green" comprehensive utilization of cellulose resources has drawn much attention from the governments and researches (Šimkovic, 2008; Varma, Kennedy, & Galgali, 2004; Wu, Wang, Li, Li, & Wang, 2009).

The all-cellulose composites composed of ramie fibers embedded in a matrix of regenerated cellulose, which was first introduced by Nishino, Matsuda, and Hirao (2004), had excellent mechanical properties and thermal performance. Subsequently, many all-cellulose composites have been reported for the creation of advanced materials with the essential advantages as being a biobased and biodegradable materials (Duchemin, Newman, & Staiger, 2009; Gindl & Keckes, 2005; Han & Yan, 2010; Nishino & Arimoto, 2007; Qi, Cai, Zhang, & Kuga, 2009; Soykeabkaew, Arimoto, Nishino, & Peijs, 2008; Soykeabkaew, Sian, Gea, Nishino, & Peijs, 2009; Zhao et al., 2009). These preceding researches on the all-cellulose composites further emphasis the "green" comprehensive utilization of cellulose resources.

In our previous work, we found that the hydroxyl functionalized ionic liquid 1-(2-hydroxylethyl)-3-methyl imidazolium chloride (denoted as [HeMIM]Cl) shows excellent solubility for alkaline cellulose with the dissolubility of 5–7%, and slightly solubility for cellulose without activating with NaOH aqueous solution (Luo, Li, & Zhou, 2005). The distinctly selective solubility of functionalized ionic liquid offers the possibility for the preparation of all-cellulose composite through a solution processing. Now, based on our previous work on dissolution of cellulose with ionic liquid, we wish herein to report the preparation of green all-cellulose composites by adding cellulose nanocrystals to the cellulose ionic liquid solution. In addition, the characterization for structure, morphologies, optical, the mechanical and thermal properties of the composites was also performed.

* Corresponding author at: Department of Chemistry, Jinan University, 601, Huangpu Avenue West, Guangzhou 510632, Guangdong, China.
Tel.: +86 20 85228537; fax: +86 20 85228537.
E-mail address: tlyq@jnu.edu.cn (Y.-Q. Li).

0144-8617/$ – see front matter © 2010 Elsevier Ltd. All rights reserved.
doi:10.1016/j.carbpol.2010.11.050

2. Experimental

2.1. Materials

The ionic liquid was synthesized according to the method reported in the literature (Branco, Rosa, Ramos, & Afonso, 2002). Pretreated microcrystalline cellulose (PMCC) was obtained by the procedure according to the literatures (Oh et al., 2005; Široký, Blackburn, Bechtold, Taylor, & White, 2010). All other chemicals were of analytical grade and purchased from commercial sources without any pretreatment.

2.2. Preparation of NCC suspension

NCC suspension was prepared by the modified method according to the literature (Bai, Holbery, & Li, 2009; Ruiz, Cavaille, Dufresne, Gerard, & Graillat, 2000; Samir, Alloin, Sanchez, Kissi, & Dufresne, 2004; Siqueira, Bras, & Dufresne, 2009). MCC powder (5.0 g) was hydrolyzed by sulfuric acid (44 g, 60 wt%) for 4 h at 50 °C with continuous stirring. The hydrolysis was quenched by adding a large amount of water (250 ml) and centrifuged (4000 rpm) (KDC-40, Anhui ustc zonkia scientific instruments co., Ltd., China) for 15 min at room temperature. Then the supernatant was decanted. After that, water (250 ml) was added to the precipitate and the mixture was further sonicated for 15 min to form a new suspension. This centrifugation and sonicated process were further repeated for several times until the suspension existed with good dispersion and stability. After the newly NCC suspension was dialyzed in running water until the pH reached a constant value, the resulted NCC was stored in ionic liquid ([HeMIM]Cl).

2.3. The dissolubility and storage of NCC in [HeMIM]Cl

A certain amount of ionic liquid was added to a quantitative NCC suspension obtained above and concentrated in a rotary evaporator at 70 °C. After most of the water was distilled out, the mixture was cooled to 50 °C, and the residual water was further excluded in vacuum. At last, the resulted NCC suspended in ionic liquid at ambient temperature was obtained and stored for further use. The solid content of NCC in the ionic liquid was determined by gravimetrical method. The results showed that the dissolubilities of NCC in [HeMIM]Cl are 0.43, 0.17 and insoluble at corresponding temperatures of 70, 60 and 50 °C, which indicated the storage of NCC in the ionic liquid at room temperature was a perfect way.

2.4. Preparation of all-cellulose composites

The clear viscous cellulose ionic liquid solution (3 wt%) can be easily prepared by the addition of PMCC (0.45 g) to the preheated ionic liquid [HeMIM]Cl (15.0 g) at 85 °C with strong stirring for 2 h. After the solution cooled to 50 °C, a certain amount of NCC stored in ionic liquid (solid content, 3.68%) was added and stirred for 10 min. The resulted almost transparent suspension was spread in a petri dish with the diameter of 7.5 cm to give a *ca.* 2 mm thick layer. The composite gel was slowly formed, and further kept in the ambient temperature for 2 days. Then, the composite gel was washed with running deionized water to remove the ionic liquid and dried in air at ambient temperature to afford all-cellulose composite film. The NCC contents of 0, 5, 10, 15, 20 and 25 wt% were denoted as Com-N0, Com-N5, Com-N10, Com-N15, Com-N20 and Com-N25 respectively.

2.5. Measurements and characterization

2.5.1. X-ray diffraction studies

The X-ray diffraction patterns with CuKα radiation (λ = 1.5406 Å) at 36 kV and 20 mA were recorded in the range of $2\theta = 5–40^\circ$ with an X-ray diffraction diffractometer (MSAL-XRD2, Bragg Science and Technology Co, Ltd., Beijing). The samples were mounted on a holder, and the proportional counter detector was set to collect data at a rate of $2\theta = 1^\circ\,\mathrm{min}^{-1}$ with increments of 0.01° for 2θ values. All samples were cut into particle-like size to erase the influence of the crystalline orientation. The crystalline structure was attributed according to the authoritative data. The total degree of crystallinity was estimated by the ratio of the crystalline scattering versus total scattering, and the crystallinity of individual crystal was estimated by the ratio of the individual crystalline scattering versus total scattering (Liu, Yu, & Huang, 2005; Smole et al., 2003), the formula as follows:

$$\mathrm{Cr} = \frac{S_\mathrm{I} + S_\mathrm{II}}{S_\mathrm{I} + S_\mathrm{II} + S_a} \times 100\% \quad (1)$$

$$\mathrm{Cr_I} = \frac{S_\mathrm{I}}{S_\mathrm{I} + S_\mathrm{II} + S_a} \times 100\% \quad (2)$$

$$\mathrm{Cr_{II}} = \frac{S_\mathrm{II}}{S_\mathrm{I} + S_\mathrm{II} + S_a} \times 100\% \quad (3)$$

$$\frac{\mathrm{Cr_I}}{\mathrm{Cr_{II}}} = \frac{S_\mathrm{I}}{S_\mathrm{II}} \quad (4)$$

where Cr is the crystallinity of overall nanocomposite films; $\mathrm{Cr_I}$ is the crystallinity of cellulose I in the composites; $\mathrm{Cr_{II}}$ is the crystallinity of cellulose II in the composites; S_I is the integrated area of cellulose I crystal peaks; S_II is the integrated area of cellulose II crystal peaks; S_a is the integrated amorphous area of cellulose composites. Individual crystal reflection peaks and the amorphous background were extracted by the Peak-Fitting process of the integrated diffraction intensity profile. Background intensity was subtracted before Peak-Fitting. Each intensity spectrum was fitted by employing a Gaussian function as the peak profile (Chen, Jakes, & Foreman, 2004; Qi et al., 2009).

2.5.2. Thermal analysis

Thermal gravimetric analysis (TGA) was carried out by using thermogravimetric analysis equipment (SDT Q600, TA, America). The nanocomposites were ground into powder, and *ca.* 15 mg of the powder was placed in a platinum pan and heated from 30 to 600 °C at a rate of $10\,^\circ\mathrm{C\,min}^{-1}$ in nitrogen atmosphere.

2.5.3. Optical transmission measurements

Optical transmittance (T_r) of the nanocomposite films were measured with a visible spectral photometer (721, Jinghua, China) at the wavelength of 800 nm (Qi et al., 2009). The transmittance of a glass plate with 1 mm thickness was taken as a reference. The thickness of the composites is about 40 μm.

2.5.4. SEM and TEM

Scanning electron microscopy (SEM) (XL-30ESEM, Philips, Holland) was used to observe the surfaces and fractured surfaces of composites by using an accelerating voltage of 20 kV. The fractured surfaces were observed directly after mechanical testing, and the samples were coated with gold to facilitate the SEM observation.

Transmission electron micrograph (TEM) of NCC was performed by using a JEM-100CX II Transmission Electron Microscope (JEOL Ltd., Japan). In brief, TEM sample was prepared by deposition of a drop of diluted suspension of nanocrystalline cellulose on a carbon-coated grid (aqueous dispersions), and the sample was stained with a 2 wt% solution of uranyl acetate.

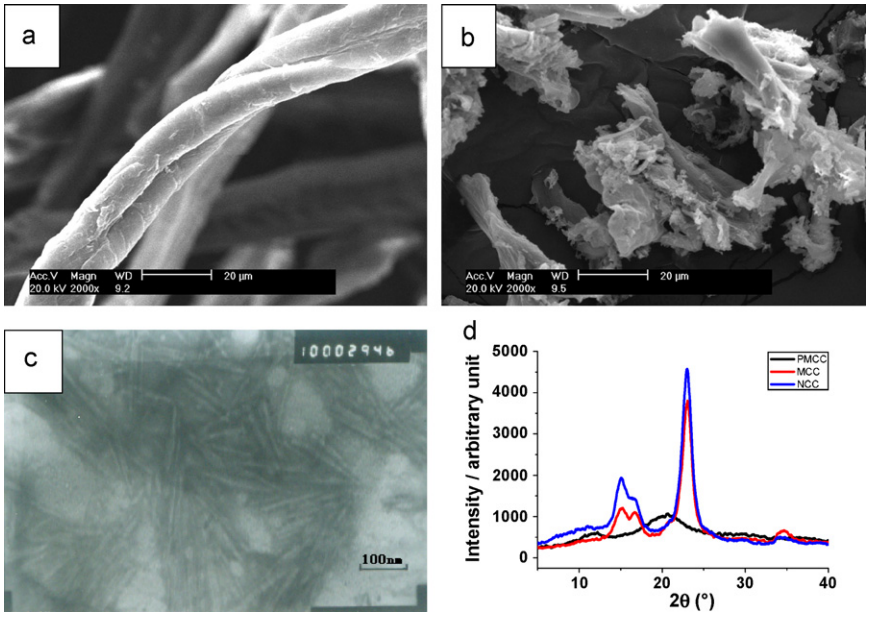

Fig. 1. SEM of MCC (a) and PMCC (b); TEM of NCC (c); XRD patterns of MCC, PMCC, and NCC (d).

2.5.5. Mechanical properties measurement

The tensile strength (σb) and elongation at break (εb) of the films were measured on a universal testing machine (AG-1, Shimadzu, Japan) at a speed of 1 mm/min. The distance between the jaws was set at 10 mm. Nanocomposite films were cut in strips about 40 μm thick, 8 mm wide and 5 cm long, and then stored at 55 ± 1% R.H. and 20 ± 1 °C for 4 days.

3. Results and discussion

3.1. Morphologies and structure of microcrystalline cellulose, alkaline cellulose, and nanocrystalline cellulose

[HeMIM]Cl, a hydroxyl-functionalized ionic liquid, has excellent dissolubility to alkaline cellulose (PMCC). The morphology and structure of the original cellulose were significantly changed (Fig. 1a, b and d) after treated by NaOH solution. The original cellulose was cellulose I crystal, and the alkaline cellulose (PMCC) was the cellulose II crystal (Han & Yan, 2010; Oh et al., 2005; Schenzel, Almlöf, & Germgård, 2009).

The NCC owned the same structure as MCC (Fig. 1d), and displayed a needle-like morphology (Fig. 1c) with length (L) and diameter (D) were 150 × 15 nm, respectively. The average aspect ratio (L/D) was about 10.

3.2. Structure, morphologies and properties of nanocomposite films

These nanocomposites were referred to "composites" because they owned the regenerated cellulose as matrix and the cellulose I crystallites as the "filler". Although matrix and filler are chemically identical, the term "composite" was considered appropriate since the two components exhibit different structures and different mechanical properties (Eichhorn & Davies, 2006; Langan, Sukumar, Nishiyama, & Chanzy, 2005; O'Sullivan, 1997).

According to the literature, the diffractogram of cellulose I displays peaks at $2\theta = 14.67^\circ$, 16.39°, and 22.53° for $(1\,\bar{1}\,0)$, $(1\,1\,0)$, and $(2\,0\,0)$ planes (Duchemin, Mathew, and Oksman, 2009; Qi et al., 2009), and cellulose II crystal has its diffraction peaks located at $2\theta = 12.1$, 19.8, and 22.0° for $(1\,\bar{1}\,0)$, $(1\,1\,0)$, and $(2\,0\,0)$ planes (Han & Yan, 2010; Qi et al., 2009; Rahatekar et al., 2009). The wide angle X-ray diffraction patterns of the nanocomposite films (Fig. 2A) revealed that two kinds of cellulose I and II coexisted in the nanocomposite films, and the amplitude of the $(2\,0\,0)$ diffraction peak obviously increased with the content of NCC from 5% to 25%, showing the content of cellulose I in the film increased with the initial proportion of the added NCC from Com-N5 to Com-N25 (from 5% to 10%). But, the $(2\,0\,0)$ plane of cellulose II crystal does not exist in Com-N0 (Fig. 2B), which is the regenerated cellulose from ionic liquid. Such changes could be seen in many literatures (Duchemin, Newman, & Staiger, 2009; Rahatekar et al., 2009). Thus, the fitted intensity curve and the diffraction peaks resolved from the X-ray spectrum of nanocomposite films do not show the $(2\,0\,0)$ plane of cellulose II (Fig. 2B (b and d)) (Rahatekar et al., 2009).

As shown in Table 1, the crystallinity of cellulose I (Cr_I) increased from 0 to 28.97% with the content of NCC increased from 0 to 25%, and the crystallinity of cellulose II (Cr_{II}) and the overall crystallinity (Cr) increased with the content of NCC in the films increased from 0 to 5% due to the NCC owned large specific surface area with very high activities. The NCC could induce the cellulose II crystallization, which further resulted in the crystallinity of cellulose II (Cr_{II}) and the overall crystallinity (Cr) increased followed up. But, interestingly, when the content of NCC increased from 5% to 20%, the overall crystallinity (Cr) of the composite films was nearly invariant in the range of 44.70–46.71%. And the crystallinity of cellulose II (Cr_{II}) decreased from 34.58 to19.99%. As mentioned above, nanocrystalline cellulose were needle-like nanoparticles having a highly active surface that could easily induce the matrix crystallizing to form the *SPECIAL PARTICLES (SPs)* which contain cellulose nanoparticle as the core and the regenerated cellulose as the shell. When increased the NCC content, the *SPs* content increased accord-

Table 1
The Cr(%), Cr_I(%), Cr_{II}(%), Cr_I(%)/Cr_{II}(%) of nanocomposite films, R^2 is correlation coefficient of Peak-Fitting.

Entry	Samples	Cr(%)	Cr_I(%)	Cr_{II}(%)	Cr_I(%)/Cr_{II}(%)	R^2
1	Com-N0	31.69	0	31.69	0	0.9986
2	Com-N5	44.70	10.12	34.58	0.29	0.9986
3	Com-N10	46.71	15.77	30.94	0.51	0.9974
4	Com-N15	46.64	19.15	27.49	0.70	0.9967
5	Com-N20	46.66	26.67	19.99	1.33	0.9974
6	Com-N25	50.88	28.97	21.89	1.32	0.9969

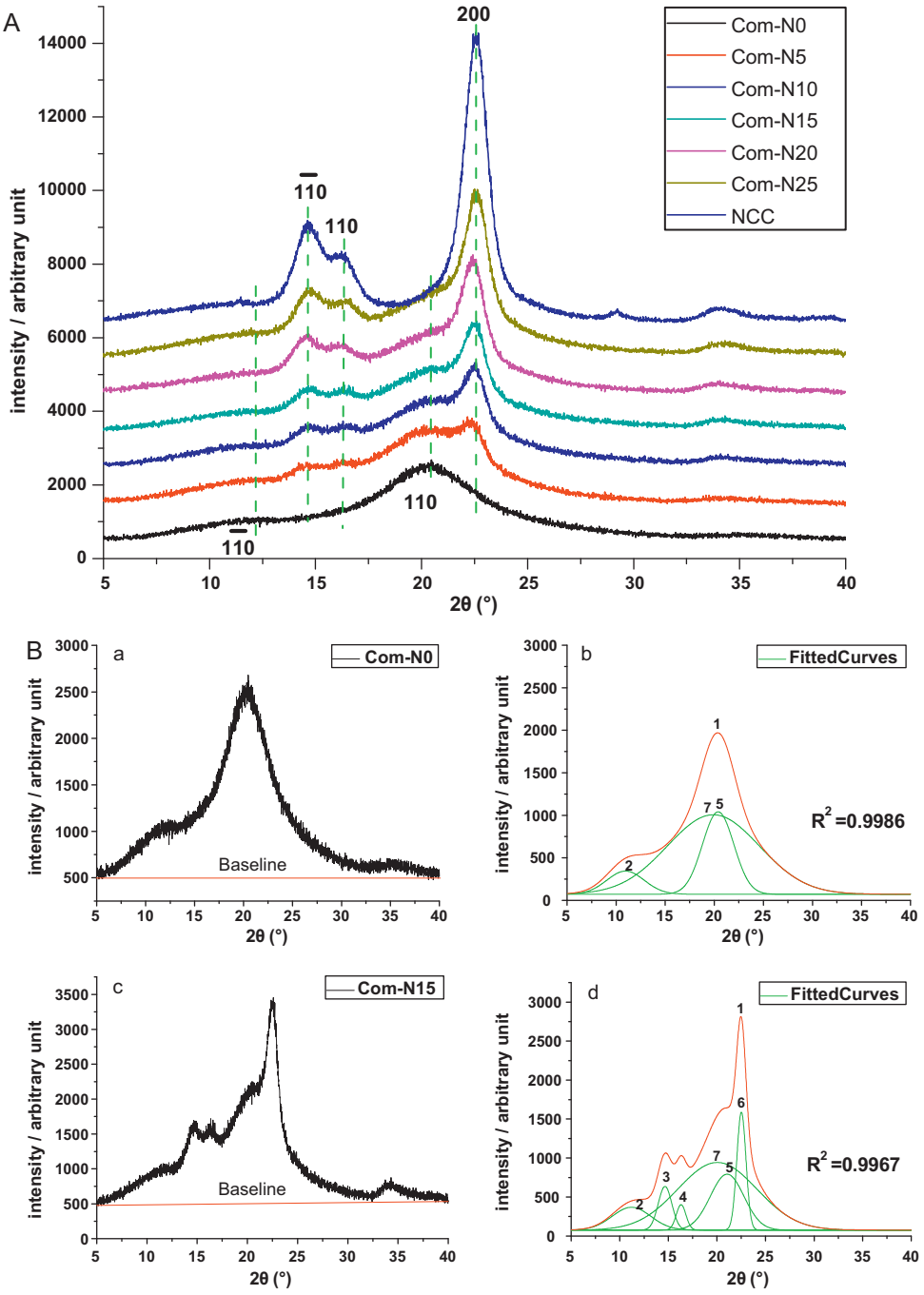

Fig. 2. (A) XRD patterns of nanocomposite films and NCC; (B) X-ray diffraction profile of samples Com-N0 and Com-N15 and corresponding peak deconvolution process to estimate the crystallinity (a and c) and the experimental intensity curve (b and d).

ingly, but the increased *SPs* content could induce their aggregates and phase separation in our finding, leading to a decrease in the crystallinity of cellulose II (Cr_{II}). Thus, the overall crystallinity was almost the same to the films containing NCC ranged from 5% to 20%. However, the content of NCC increased from 20% to 25%, the crystallinity of cellulose II (Cr_{II}) and the overall crystallinity (Cr) increased again. When the NCC concentration was high enough, the contribution of crystallization induced by NCC increased to the crystallinity, and the influence of phase separation decreased. This result was the reason for the crystallinity of cellulose II (Cr_{II}) and the overall crystallinity (Cr) increased again. The ratio of Cr_I versus Cr_{II} increased from 0 to 1.33 as the NCC content increased from 0 to 20%. Moreover, as the NCC content increased from 20% to 25%, the ratio was nearly invariant. In addition, the results of XRD for nanocomposite films also shown that keeping nanocrystalline cellulose in ionic liquid was the perfect way to keep NCC displaying a needlelike morphology and cellulose I crystal.

SEM images of the surfaces for nanocomposite films are shown in Fig. 3. The pure regenerated cellulose (Com-N0) film and the Com-N5 nanocomposite film (Fig. 3a and b) exhibited a smooth surface. It suggested that the cellulose nano-particles were embedded in the regenerated cellulose matrix because of the strong interaction between cellulose I and cellulose II. However, as the content of NCC increased from 10% to 25%, the nanocomposite films gave increasingly rough surface, indicating that certain phase separation occurred here. The particles shown on the surface of composite

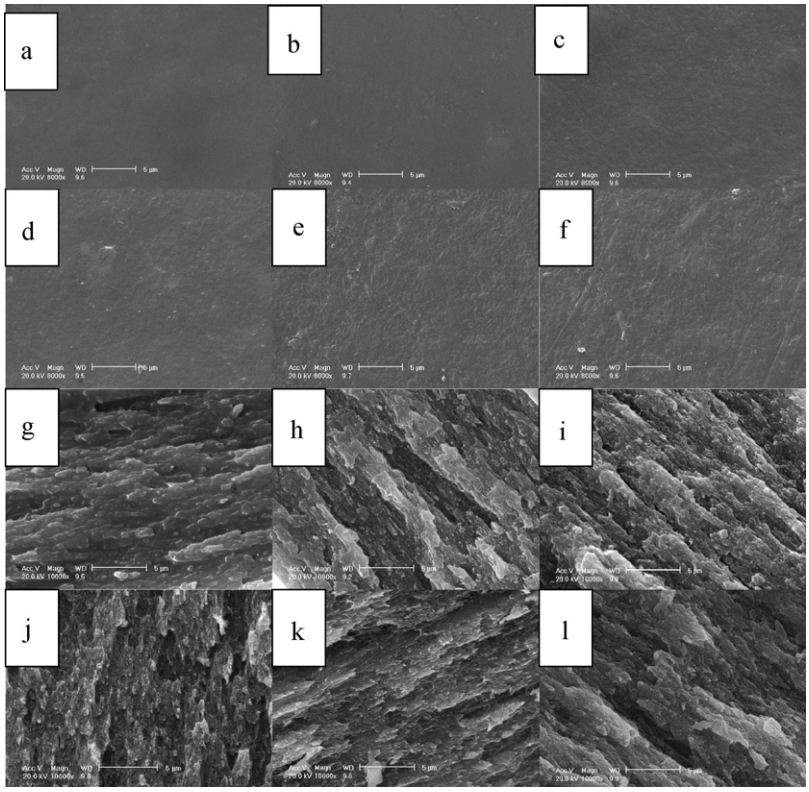

Fig. 3. The SEM images of surface (a–f) and cross-section (g–l) for all-cellulose nanocomposite films, Com-N0 (a and g); Com-N5 (b and h); Com-N10 (c and i); Com-N15 (d and j); Com-N20 (e and k); Com-N25 (f and l).

films may be the *SPs*. It suggested that the cellulose nanoparticles were embedded in the regenerated cellulose matrix because of the strong interaction between cellulose I and cellulose II.

The SEM images of fractured surfaces for the nanocomposites were shown in Fig. 3g–l. The NCC added as the filler to the cellulose matrix increased the roughness of the fractured surfaces, indicating the filler and the matrix taken on the sufficient stress transfer as the Halpin–Kardos model (Halpin & Kardos, 1972; Rusli, Shanmuganathan, Rowan, Weder, & Eichhorn, 2010) and good adhesion through the perfect interface. The results from Fig. 3 were in good agreement with the data from XRD.

The TGA curves of the composite films were shown in Fig. 4a. As Fig. 4a shows, the addition of NCC slightly decreased the water content in the films compared with the film without adding any NCC according to the weight loss from 30 °C to 100 °C. The decomposition temperatures of the nanocomposite films were shown in Table 2. As expected, the NCC could increase the thermal stability of nanocomposite films compared Com-N0 with Com-N5, this result was a good indication of the high compatibility between the filler and matrix. But, as the content of filler increased from 5% to 25%, the decomposition temperatures decreased from 304.0 °C to 294.2 °C. This was relative to the phase separation as a result of the *SPs* aggregate. Moreover, the results further supported by the conclusion from the crystallinity values and SEM of nanocomposites.

Table 2
Results of thermal gravimetric analysis (TGA), tensile strength (σb), Young's modulus (E), strain at failure (ε) and optical transmittance (T_r) of all-cellulose nanocomposite films compared to pure regenerated cellulose films.

Entry	Samples	NCC content (wt%)	T_d (°C)	σb (MPa)	E (MPa)	ε (%)	T_r (800 nm, %)
1	Com-N0	0	297.8	34.87	1103.18	13.89	99.93
2	Com-N5	5	304.0	43.62	1233.20	15.90	99.90
3	Com-N10	10	302.7	51.37	2168.24	9.63	99.89
4	Com-N15	15	300.3	51.91	2238.95	3.89	99.88
5	Com-N20	20	299.1	50.22	2913.49	2.83	99.87
6	Com-N25	25	294.2	49.24	3633.96	2.11	99.86

The transparency is a useful criterion for the miscibility of the composite elements. The optical transmittance (T_r) of the composites at a wavelength of 800 nm was shown in Table 2. The nanocomposite films embedded with the NCC from 5 to 25 wt% exhibited excellent optical transmittance, indicating perfect miscibility and compatibility. With an increase in the content of NCC, the T_r value for the composite films just decreased from 99.93 to 99.86%. But, the slight decrease in the optical transmittance could also reflect the influence of the introduction of the *SPs* on the interface structure. When the content of *SPs* was high enough, the aggregate could be formed. Thus, the particle aggregates led to the scattering caused by large particles, resulting in the decrease of T_r. These results could also explain the phenomenon shown in XRD, SEM and TGA.

The mechanical properties of the composite materials are strongly influenced by the microstructure, and they could provide important information about the internal structure of materials. Stress–strain curves of the all-cellulose composite films and pure regenerated cellulose films were shown in Fig. 4b. Nanocomposite films exhibited significant improvements due to the process of adding NCC to the cellulose matrix. The films underwent the most significant changes with a large increase in tensile strength, Young's modulus and tensile strain, indicating the filler and the matrix taken on the sufficient stress transfer (Halpin & Kardos, 1972; Rusli et al., 2010).

When the NCC content increases from 0 to 10 wt%, the tensile strength (σb) increased from 34.87 to 51.37 MPa; thereafter, the tensile behavior was nearly constant (Table 2). Obviously, the incorporation of the NCC into the cellulose matrix led to the strengthening of the materials as a result of stiffness of the nano-

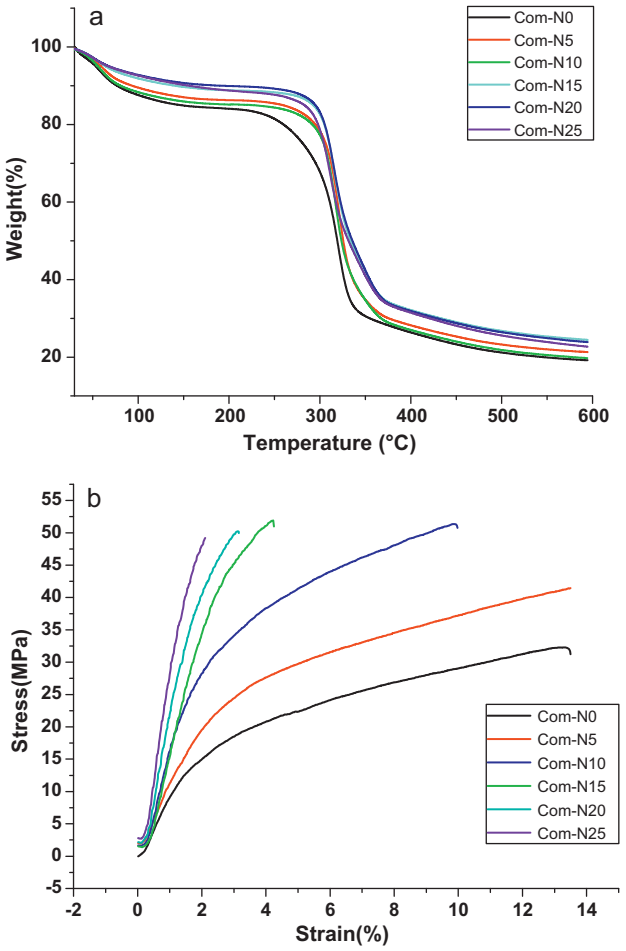

Fig. 4. (a) Thermal decomposition profiles of composite films and (b) stress–strain curves of nanocomposite films and pure regenerated cellulose films.

particles and the strong interactions between the cellulose matrix and the NCC through hydrogen bonds. However, the composites containing more than 10 wt% NCC exhibited a slight decrease in the tensile strength. Therefore, the optimal amount of NCC in the nanocomposite films should be 5–10 wt%, where a significant improvement in the thermal stability and the mechanics strength created. The increase in the NCC content led marked enhancement in Young's modulus (E), from 1103.18 MPa to 3633.96 MPa, whereas the elongation at break (εb) increased slightly from 13.89% to 15.90% as the NCC content increased from 0% to 5%. Then, the elongation at break decreased slightly from 15.90% to 2.11% as the NCC content increased from 5% to 25%.

In view of the above results, the nanocrystalline cellulose strengthened the regenerated cellulose film, because of the role of the nanocrystalline cellulose embedded in cellulose matrix. Therefore, the self-reinforcement in the cellulose films was created in the system of ionic liquid solution. The all-cellulose films reinforced with 5–10 wt% cellulose NCC possessed excellent mechanical and thermal properties compared with Com-N0.

4. Conclusions

Cellulose needle-like nano-particles with an average length of about 150 nm and diameter around 15 nm were prepared from MCC by using an aqueous sulfuric acid solution (60 wt%) and further used to reinforce regenerated cellulose. Storage of NCC in the ionic liquid at room temperature was a perfect way to keep native crystal retaining their structure and needlelike shape. The all-cellulose nanocomposite films were consisted of NCC (cellulose I) as fillers and regenerated cellulose (cellulose II) as matrix, creating the self-reinforced materials. NCC was the excellent filler for the cellulose matrix, it could improve the tensile strength, Young's modulus and the strain at failure of the cellulose materials, and it could also improve the thermal stability of cellulose composites. Moreover, the advantage of the nanocomposite film was that they were fully biobased, easily recyclable and biodegradable, and expected to be useful as biomaterials and food ingredients.

Acknowledgments

We are grateful to the National Natural Science Foundation of China (Nos. 21072077 and 20672046), the Guangdong Natural Science Foundation (Nos. 10151063201000051 and 8151063201000016) and the Department of Education of Guangdong Province (cgzhzd0709) for financial support.

References

Bai, W., Holbery, J., & Li, K. (2009). A technique for production of nanocrystalline cellulose with a narrow size distribution. *Cellulose*, *16*(3), 455–465.
Branco, L. C., Rosa, J. N., Ramos, J. J. M., & Afonso, C. A. M. (2002). Preparation and characterization of new room temperature ionic liquids. *Chemistry-A European Journal*, *8*(16), 3671–3677.
Chen, R., Jakes, K. A., & Foreman, D. W. (2004). Peak-fitting analysis of cotton fiber powder X-ray diffraction spectra. *Journal of Applied Polymer Science*, *93*(5), 2019–2024.
Duchemin, B. J. C., Mathew, A. P., & Oksman, K. (2009). All-cellulose composites by partial dissolution in the ionic liquid 1-butyl 3-methylimidazolium chloride. *Composites Part A*, *40*(12), 2031–2037.
Duchemin, B. J. C., Newman, R. H., & Staiger, M. P. (2009). Structure–property relationship of all-cellulose composites. *Composites Science and Technology*, *69*(7–8), 1225–1230.
Eichhorn, S. J., & Davies, G. R. (2006). Modelling the crystalline deformation of native and regenerated cellulose. *Cellulose*, *13*(3), 291–307.
Fink, H.-P., Weigel, P., Purz, H. J., & Ganster, P. J. (2001). Structure formation of regenerated cellulose materials from NMMO-solutions. *Progress in Polymer Science*, *26*(9), 1473–1524.
Gindl, W., & Keckes, J. (2005). All-cellulose nanocomposite. *Polymer*, *46*(23), 10221–10225.
Halpin, J. C., & Kardos, J. L. (1972). Moduli of crystalline polymers employing composite theory. *Journal of Applied Physics*, *43*(5), 2235–2241.
Han, D., & Yan, L. (2010). Preparation of all-cellulose composite by selective dissolving of cellulose surface in PEG/NaOH aqueous solution. *Carbohydrate Polymers*, *79*(3), 614–619.
Langan, P., Sukumar, N., Nishiyama, Y., & Chanzy, H. (2005). Synchrotron X-ray structures of cellulose Ib and regenerated cellulose II at ambient temperature and 100 K. *Cellulose*, *12*(6), 551–562.
Liu, R., Yu, H., & Huang, Y. (2005). Structure and morphology of cellulose in wheat straw. *Cellulose*, *12*(1), 25–34.
Luo, H.-M., Li, Y.-Q., & Zhou, C.-R. (2005). Study on the dissolubility of the cellulose in the functionalized ionic liquid. *Polymer Materials Science and Engineering*, *21*(2), 233–240.
Nishino, T., & Arimoto, N. (2007). All-cellulose composite prepared by selective dissolving of fiber surface. *Biomacromolecules*, *8*(9), 2712–2716.
Nishino, T., Matsuda, I., & Hirao, K. (2004). All-cellulose composite. *Macromolecules*, *37*(20), 7683–7687.
Oh, S. Y., Yoo, D. I., Shin, Y., Kim, H. C., Chung, Y. S., Parkd, W. H., et al. (2005). Crystalline structure analysis of cellulose treated with sodium hydroxide and carbon dioxide by means of X-ray diffraction and FTIR spectroscopy. *Carbohydrate Research*, *340*(15), 2376–2391.
O'Sullivan, A. C. (1997). Cellulose: The structure slowly unravels. *Cellulose*, *4*(3), 173–207.
Qi, H., Cai, J., Zhang, L., & Kuga, S. (2009). Properties of films composed of cellulose nanowhiskers and a cellulose matrix regenerated from alkali/urea solution. *Biomacromolecules*, *10*(6), 1597–1602.
Rahatekar, S. S., Rasheed, A., Jain, R., Zammarano, M., Koziol, K. K., Windle, A. H., et al. (2009). Solution spinning of cellulose carbon nanotube composites using room temperature ionic liquids. *Polymer*, *50*(19), 4577–4583.
Ruiz, M. M., Cavaille, J. Y., Dufresne, A., Gerard, J. F., & Graillat, C. (2000). Processing and characterization of new thermoset nanocomposites based on cellulose whiskers. *Composite Interfaces*, *7*(2), 117–131.
Rusli, R., Shanmuganathan, K., Rowan, S. J., Weder, C., & Eichhorn, S. J. (2010). Stress-transfer in anisotropic and environmentally adaptive cellulose whisker nanocomposites. *Biomacromolecules*, *11*(3), 762–768.
Samir, M. A. S. A., Alloin, F., Sanchez, J., Kissi, N. K., & Dufresne, A. (2004). Preparation of cellulose whiskers reinforced nanocomposites from an organic medium suspension. *Macromolecules*, *37*(4), 1386–1393.

Schenzel, K., Almlöf, H., & Germgård, U. (2009). Quantitative analysis of the transformation process of cellulose I → cellulose II using NIR FT Raman spectroscopy and chemometric methods. *Cellulose*, *16*(3), 407–415.

Schurz, J. (1999). "Trends in Polymer Science". A bright future for cellulose. *Progress in Polymer Science*, *24*(4), 481–483.

Šimkovic, I. (2008). What could be greener than composites made from polysaccharides? *Carbohydrate Polymers*, *74*(4), 759–762.

Siqueira, G., Bras, J., & Dufresne, A. (2009). Cellulose whiskers versus microfibrils: Influence of the nature of the nanoparticle and its surface functionalization on the thermal and mechanical properties of nanocomposites. *Biomacromolecules*, *10*(2), 425–432.

Široký, J., Blackburn, R. S., Bechtold, T., Taylor, J., & White, P. (2010). Attenuated total reflectance Fourier-transform infrared spectroscopy analysis of crystallinity changes in lyocell following continuous treatment with sodium hydroxide. *Cellulose*, *7*(1), 103–115.

Smole, M. S., Peršin, Z., Kreže, T., Kleinschek, K. S., Ribitsch, V., & Neumayer, S. (2003). X-ray study of pre-treated regenerated cellulose fibres. *Materials Research Innovations*, *7*(5), 275–282.

Soykeabkaew, N., Arimoto, N., Nishino, T., & Peijs, T. (2008). All-cellulose composites by surface selective dissolution of aligned ligno-cellulosic fibres. *Composites Science and Technology*, *68*(10–11), 2201–2207.

Soykeabkaew, N., Sian, C., Gea, S., Nishino, T., & Peijs, T. (2009). All-cellulose nanocomposites by surface selective dissolution of bacterial cellulose. *Cellulose*, *16*(3), 435–444.

Takagi, H., & Asano, A. (2008). Effects of processing conditions on flexural properties of cellulose nanofiber reinforced "green" composites. *Composites Part A: Applied Science and Manufacturing*, *39*(4), 685–689.

Varma, A. J., Kennedy, J. F., & Galgali, P. (2004). Synthetic polymers functionalized by carbohydrates: A review. *Carbohydrate Polymers*, *56*(4), 429–445.

Wu, R.-L., Wang, X.-L., Li, F., Li, H.-Z., & Wang, Y.-Z. (2009). Green composite films prepared from cellulose, starch and lignin in room-temperature ionic liquid. *Bioresource Technology*, *100*(9), 2569–2574.

Zhao, Q., Yam, R. C. M., Zhang, B., Yang, Y., Cheng, X., & Li, R. K. Y. (2009). Novel all-cellulose ecocomposites prepared in ionic liquids. *Cellulose*, *16*(2), 217–226.